IEEE Access
Multidisciplinary ⋮ Rapid Review ⋮ Open Access Journal

Received 31 January 2023, accepted 14 February 2023, date of publication 22 February 2023, date of current version 27 February 2023.

Digital Object Identifier 10.1109/ACCESS.2023.3247519

RESEARCH ARTICLE

Wireless Technology Identification Employing Dynamic Mode Decomposition Modeling

AHMED ELSEBAAY AND HAZEM H. REFAI, (Member, IEEE)
Department of Electrical and Computer Engineering, The University of Oklahoma, Tulsa, OK 74135, USA
Corresponding author: Ahmed Elsebaay (ahmed.m.elsebaay-1@ou.edu)

ABSTRACT Significant growth in broadband wireless services, as well as ever-increasing demand on the spectrum caused by the Internet of Things (IoT) have overstretched limited available spectrum space for wireless services. Heterogeneous wireless networks (HetNets)—wherein multiple wireless technologies (e.g., Wi-Fi, Bluetooth, Zigbee, LTE, and GSM) coexist and share spectrum—are a promising solution for enhancing spectrum sharing. An essential element in developing coexistence protocols is correctly identifying wireless technologies anticipated to share spectrum and to shift users between available wireless technologies in an effort to optimize spectrum usage and minimize interference. For the coexistence research reported in this paper, we analyzed the performance of our developed novel algorithm based on dynamic mode decomposition (DMD) mathematical modeling to identify and differentiate among various wireless technologies. More specifically, our technique identified GSM and LTE signals in the cellular domain, IEEE802.11n, ac, and ax in the Wi-Fi domain, as well as Bluetooth and Zigbee. The proposed DMD-based technique identifies the time domain signature of a signal by capturing embedded periodic features transmitted within the signal. Performance and accuracy were tested and validated using an experimental dataset collected for various time series, and raw-power measurements of the targeted technologies. Results showed that the developed DMD-based algorithm can differentiate and classify individual and coexisting wireless signals with high accuracy —greater than 90% for most cases. Furthermore, only a short time— less than one second—is required for identifying a signal and enabling implementation in real-time practical networks. The advantage of the developed technique over comparable techniques is lower complexity (i.e., shorter processing and training time, no channel estimation, no time/frequency synchronization, and no need for long observation-time intervals).

INDEX TERMS Dynamic mode decomposition, wireless coexistence, wireless identification.

I. INTRODUCTION

Escalating traffic demands coincide with significant growth in broadband wireless services. Vast connectivity and the Internet of Things (IoT) are causes for a consistently overstretched spectrum space [1], [2], thus, increasing spectrum scarcity. Constrained licensed spectrum resources are simply unable to meet the ever-rising demand [1], [3]. Scarcity and high cost of licensed spectrum cause wireless technologies (e.g., Wi-Fi, ZigBee, and Bluetooth) to share spectrum in unlicensed bands [4]. The ISM band is one such unlicensed and unrestricted band, and many technologies try to coexist in it [5]. This trend has led to overutilization and congestion, which, in turn, has caused various levels of interference among coexisting technologies.

Heterogeneous wireless networks (HetNets) employing smart cognitive radio devices have been introduced as an effective solution to enhance network capacity, data rate, coverage, and spectrum resource utilization. HetNets are composed of several coexisting wireless technologies sharing wireless spectrum [1], [6], [7]. Ensuring effective coexistence across suitable wireless technologies is imperative.

Wireless technologies must be identified within a frequency range in order for intelligent cognitive radio devices to analyze spectrum occupancy, identify available channels, and model interference while attempting to coexist. Only then can communication be effective and successful [5].

The associate editor coordinating the review of this manuscript and approving it for publication was Hosam El-Ocla.

A. RELATED WORK

Wireless signals are identified as likelihood-based (LB) and feature-based (FB). Conventional LB methods are based on calculating maximum average probability for proper identification. Recent FB schemes rely on capturing common features shared among similar signal types. Comparing LB methods with FB methods shows that although the latter has suboptimal performance, FB has a simpler implementation, lower computational complexity, and relative robustness for modeling mismatches among various operation cases [1], [8]. FB algorithms are based on wavelets, cumulative distribution functions (CDF), second-order cyclostationarity, machine learning (ML), and deep learning (DL). Each technique is briefly described in the following sections and ordered from oldest to most recent schemes.

1) WAVELET-BASED ALGORITHMS

References [9] and [10] introduced a wavelet-based algorithm for identifying GSM and UMTS signals relying on differences in their respective modulation schemes. The algorithm applied wavelet transform to extract transient behaviors within signals resulting from modulation types, and then utilizes template matching in the wavelet transform domain for identification.

2) SECOND-ORDER CYCLOSTATIONARITY-BASED ALGORITHMS

Reference [11] utilized a second-order cyclostationarity-based algorithm to detect and identify cyclic patterns of GSM, wideband code division multiple access (WCDMA), and orthogonal frequency division multiplexing (OFDM) modulated signals. Cyclostationarity generated by cyclic prefix, preamble, and pilot signals were exploited by [1] to classify GSM, LTE, and CDMA signals utilizing fast Fourier transform (FFT), autocorrelation function (ACF), power spectral density (PSD), and spectral correlation function (SCF) as features for support vector machines (SVM). Reference [12] successfully employed a cyclostationarity-based technique to classify LTE and GSM signals based on their perspective pilot signals. Researchers also investigated the effect of signal-to-noise ratio (SNR) and observation time on identification accuracy. A classifier model developed by [7] was used for recognizing eight wireless standard signals, namely WCDMA, LTE, GSM, CDMA, Digital Enhanced Cordless Telecommunications (DECT), WLAN, Bluetooth, and Digital Video Broadcasting (DVB). The technique is based on transforming second-order cyclostationarity to SCF, and then utilizing it as an input to SVM for classification.

By utilizing hidden Markov Models to find second-order cyclic OFDM features, 802.11 a/g signals were categorized in [13]. The authors used a software-defined radio in [14] to present a combined energy detection and cyclostationarity-based technique for detecting IEEE 802.11g and IEEE 802.15.4 signals in the 2.4 GHz range. The highest accuracy was 90% for signals with 1.6 dB SNR.

3) CDF-BASED ALGORITHMS

CDF-based algorithms mitigate the primary limiting issues in wavelet-based and cyclostionarity-based algorithms by processing signals that require a shorter observation interval and can tolerate signal SNR variation. Researchers in [15] introduced a novel identification method for distinguishing GSM signals from LTE signals. Amplitude of the observed signal samples was employed to extract technology-based features using statistics and signal structures obtained from time and frequency domains. A Kolmogorov-Smirnov (K-S) test was then used to develop a decision principle. The same technique was used by [16] to identify LTE, UMTS, GSM, and CDMA2000 networks.

4) DL-BASED ALGORITHMS

DL-based has been recently introduced as a useful method for classifying wireless signals. Convolutional neural networks (CNN) are the most popular DL architectures exploiting both modulation and wireless technology recognition [2]. Highlighting the most recent work in the DL area, researchers in [17] and [18] chiefly constructed classification models based on CNN to process time series signals for GSM, UMTS, and LTE. Authors in [18] enhanced the trained model by utilizing both image and vector representations of the signals. The model achieved high accuracy for classifying signals, including GSM and LTE, with additive white Gaussian noise (AWGN) and Rayleigh fading channels used to identify UMTS, LTE, and 5G signals simulated by MATLAB LTE and 5G toolboxes. Reference [19] proposed a DL-based intelligent recognition method for identifying unlicensed band LTE and Wi-Fi signals generated in a laboratory environment. CNN and recurrent neural network (RNN) models were trained using in-phase and quadrature (IQ) signals.

Reference [20] used a CNN-based approach for classifying 802.11 b/g, 802.15.4, and 802.15.1 signals that coexist in 2.4GHz unlicensed bands. For SNR greater than or equal to 5 dB, the model's accuracy was greater than 95%. Authors in [21] classified LTE, WiFi, and DVB-T technologies that share the same ISM band using Received signal strength indication (RSSI), IQ samples, and spectrogram features. A CNN model was employed in [5] to distinguish individual and coexisting 802.11n, Bluetooth, and Zigbee signals using frequency domain features. The model was trained using power-frequency measurements taken from the IQ components recorded at various SNR levels. Researchers compared different ML models' categorization accuracy. Results revealed that for signals with an SNR higher than 15dB, CNN had the highest classification accuracy— greater than 90%.

Convolutional denoising autoencoders (CDAEs) were used in a similar study published in [22] to recover distorted spectrograms before categorizing signals with CNN. The model achieved 91% accuracy when identifying IEEE 802.11a, IEEE 802.11n, IEEE 802.11ax, IEEE 802.11ac, and unlicensed LTE signals. A WaveNet model-adapted neural network was created by authors in [23] to distinguish between 802.11n, 802.11ac, and 802.11ax Wi-Fi signals. Raw power

time series data were gathered for both standalone and coexisting signals at different throughputs. The approach had a high classification accuracy between 90 and 98%. Ten wireless technologies, including Wi-Fi, ZigBee, and Bluetooth, were classified in the 2.4GHz ISM band in [24]. Experimentally, raw IQ samples were collected in an indoor lab. A DL multi-task neural architecture was created by researchers for identifying signals by their modulation properties. Reference [25] classified separate and coexisting Bluetooth, Wi-Fi, and microwave signals using a pre-trained, InceptionV3, CNN-based model. ComBlock's commercial, off-the-shelf modules generated signals in the 2.4GHz ISM band. The model's overall accuracy was 98% for 800 testing samples.

Researchers in [26] utilized CNN to identify various wireless signals based on their modulation. Constellation diagrams were generated for each signal category, and then used for training and testing several pre-trained CNN-based models, including AlexNet, VGG-16, and VGG-19. Classification accuracy was higher than 85% for signals with SNR greater than 5 dB. Accuracy was extremely low for signals with SNR less than 3 dB. An improved deep learning model (i.e., multilayer perceptron neural architecture) was proposed in [27] and [24] to classify received signals based on their modulation. Signals were classified with accuracy higher than 95% when SNR was greater than 0 dB. Researchers in [28] applied Deep Residual Network (ResNet), Convolutional Long Short Term Deep Neural Network (CLDNN), CNN, and RNN on the RadioML dataset. The models successfully classified 11 wireless technologies with SNRs ranging from −20 dB to 18 dB. AutoML was employed to reduce time for training and tuning hyper-parameters of the models. CNN accuracy was highest (85% for signals of SNR>2 dB) and RNN was lowest. Our developed DMD-based algorithms differ from those aforementioned and recent studies by two distinguishing features. First, the DMDF accuracy is independent of signal SNR. The algorithm relies on tracking oscillation frequencies for various technologies. While DMDA algorithm implements power normalization among received signals to reduce its dependence on SNR, achieving accuracies above 90%. Second, the DMD algorithms were able to track the periodic preamble transmissions within a signal under poor channel conditions. While the other algorithms track signal modulation requiring good channel conditions to achieve high accuracy.

5) ML-BASED ALGORITHMS

Although DL approaches achieve high accuracy models with the advantage of simple feature pre-processing or even raw data input, they also require large-scale training datasets, resulting in high implementation costs and large computational time. As a result, ML techniques, such as SVM in [1] and [29] and Random Forest (RF) in [8] and [30], have been widely used in related research for identifying various standards' wireless signals. Researchers have demonstrated promising results with reduced-size datasets [8]. Individual and coexisting IEEE 802.11b/g/n, 802.15.4, 802.15.1, and Bluetooth Low Energy (BLE) technologies were categorized by authors in [31] for the 2.4 GHz ISM band. They used a variety of ML algorithms, including decision trees (DT), RF, and SVM, demonstrating 90–97% identification accuracy for signals with SNR greater than 0dB.

The FB approaches detailed above are based on extracting specific features from a certain signal, and then identifying the signal using a classification model. The classification decision is performed by analyzing the probability distribution function (PDF) of the feature vectors or minimizing the error between the calculated and estimated values. These approaches have the advantages of being a) simple to implement and b) proven to provide near-optimal performance. However, they are sensitive to noise level and/or might require prior information about targeted signals [8]. Cyclostationarity-based and wavelet-based schemes require long observation intervals. The same is true for DL-based algorithms. Additionally, DL algorithms are highly computationally complex and require increased time to converge. ML-based algorithms require further data preprocessing and rely on expert knowledge for understanding the data structure. Table 1 provides a summary of the recent algorithms proposed in the literature and the pros and cons of each technique.

B. RESEARCH CONTRIBUTION AND PAPER ORGANIZATION

In this paper, we developed two novel techniques for wireless technology identification based on DMD (i.e., a data-driven modeling algorithm). We proposed a DMD mode amplitude-based identification (DMDA) and a DMD mode oscillation frequency-based identification (DMDF) technique for extracting the unique periodic features embedded in various wireless standard signals. The proposed algorithms process raw power-measured signals, capturing specifically embedded periodic features within the targeted signals represented in pilot, preamble, synchronization, and control signals. The classification was performed for both individual (or baseline) and different coexistence scenarios. To improve user experiences with signal quality and boost coexistence and spectrum utilization, our schemes offer a strategy that can be practically applied to smart radio devices within contemporary HetNets. Based on outcomes, our methods for using DMD in wireless signal detection provide the following benefits over equivalent methods:

1) Long observation intervals are not necessary. Fewer signal samples are required for the technique to operate.
2) Truncated singular value decomposition (SVD) is a technique used by DMD that significantly reduces processing time and computational complexity.
3) When processing signals, there is no need for time synchronization.
4) Identification and classification are direct, one-step processes that do not require further classification techniques to extract features.

5) Accuracy is not affected by signal power and SNR variations, as DMDA normalizes signal power before classification, and DMDF relies on comparing oscillation frequencies.
6) The techniques can identify signals in real time.

The balance of this paper is structured as follows. The methodology and mathematical foundation of the identification algorithms are described in Section II. Section III describes the embedded periodic features in the standard PHY frame format for different wireless technologies. The experimental setup and dataset details are described in Section IV. The results, algorithm evaluation, and validation are reported in Section V. Finally; section VI concludes the paper.

II. METHODOLOGY

A DMD data-driven modeling algorithm forms the foundation of the identification schemes created for the research reported in this paper. DMD represents a perfect combination of proper orthogonal decomposition (POD), and Fourier transforms in the time domain [32]. DMD breaks down a dynamical system into a number of approximated Koopman modes. In addition to energy (or amplitude), DMD modes are ranked by detected dynamics (or frequency). As a result, each mode has a distinct amplitude and frequency property [33]. Without relying on presumptions, DMD finds dominant frequencies that show repeating periodicity in signals or systems [34], [35]. We created two wireless technology identification schemes: 1) DMD mode amplitude-based identification (DMDA) and 2) DMD mode oscillation frequency-based identification (DMDF). The methods identify and distinguish between various wireless technologies coexisting in a heterogeneous network utilizing resulting DMD eigenvalues and eigenvectors (i.e., DMD modes).

A. THE STANDARD DMD ALGORITHM

Assume a nonlinear dynamical system is approximated by a best linear-fit operator A, which evolves state X forward in time for each k = 1, 2,…..,n-1

$$X_{k+1} = AX_k \tag{1}$$

Operator $A \epsilon R^{nxn}$ is the best linear fit operator, and it approximates Koopman operator. This operator satisfies (1) and represents the solution of a Frobenius norm least-squares optimization between the one-step future state X_{k+1} and the expected future state AX_k:

$$min \| X_{k+1} - AX_k \| \tag{2}$$

Consequently, we can write the equation in data matrix format as

$$X' = AX \tag{3}$$

where, X is the temporal data matrix and X' is the data matrix advanced one step Δt in the future [32].

The standard DMD can be formulated in the following steps:

Step 1: Compute the SVD of X:

$$X = U_r \Sigma_r V_r^* \tag{4}$$

where, U_r and V_r consist of r left/right singular vectors corresponding to the r dominant singular values. Σ_r is the singular values diagonal matrix. The non-negative diagonal elements of Σ_r are the r singular values denoted by σ_i, which are sorted in descending order to satisfy the truncation approximation.

Step 2: Calculate the reduced order matrix $\tilde{A} \epsilon R^{nxn}$. Matrix $\tilde{A}$ describes a low-dimensional, approximated linear model of the system:

$$\tilde{A} = U_r^* A U_r = U_r^* X' V_r \Sigma_r^{-1} \tag{5}$$

Step 3: Find the eigenvectors and eigenvalues of $\tilde{A}$ by solving the equation:

$$\tilde{A} W = \Lambda W \tag{6}$$

where, the columns of W are the eigenvectors and Λ is a diagonal matrix containing the corresponding eigenvalues λ_k of both A and $\tilde{A}$.

Step 4: Compute the eigenvectors of A (i.e., DMD modes), which are given by column vectors of matrix Φ:

$$\Phi = U_r W \tag{7}$$

B. DATA FORMATTING

Available raw power signals are prepared as algorithm input during this stage. As a mapping procedure, we used the Hankel matrix staking method [32], [36] to transform a univariate time series data with length n into a multidimensional matrix of size (m x k). The form in (1) describes a time series signal of length n and fixed sampling time Δt:

$$Y = [y_1\ y_2\ y_3 \dots\ y_n] \tag{8}$$

We created data matrix X and its related one-time step evolution data matrix X' using the Hankel matrix stacking approach:

$$X = \begin{bmatrix} y_1 & y_2 & y_3 & \cdots & y_k \\ y_2 & y_3 & y_4 & \cdots & y_{k+1} \\ \vdots & \vdots & \vdots & \vdots & \vdots \\ y_m & y_{m+1} & y_{m+2} & \cdots & y_{m+k-1} \end{bmatrix} \tag{9}$$

$$X' = \begin{bmatrix} y_2 & y_3 & y_4 & \cdots & y_{k+1} \\ y_3 & y_4 & y_5 & \cdots & y_{k+2} \\ \vdots & \vdots & \vdots & \vdots & \vdots \\ y_{m+1} & y_{m+2} & y_{m+3} & \cdots & y_{m+k} \end{bmatrix} \tag{10}$$

such that

$$m = n - k + 1 \tag{11}$$

where, m is the number of stacks. We defined column vectors of data matrices as snapshots, such that k is the number of snapshots.

TABLE 1. Recent Wireless technologies identification schemes.

Model	Cyclostationarity-based	CDF-based	ML-based	DL-based
Identified technologies	GSM, LTE, CDMA, WCDMA, OFDM, WLAN, Bluetooth	GSM, LTE, UMTS, CDMA2000	2ASK, 4ASK, QPSK, 2FSK and 4FSK ITS-G5, LTE-V2X, NR-V2X,BPSK, MSK, OFDM, IEEE 802.11b/g/n, 802.15.4, 802.15.1, and BLE	GSM, LTE, UMTS, IEEE 802.11a/ac/b/g/n/ax, 802.15.4, 802.15.1, DVB-T, Bluetooth, and ZigBee
Employed Features	FFT spectrum, ACF, PSD, SCF, and cyclic frequency	CDF function	High order cumulants, Instantaneous Frequency, SCF, burst length, burst mean power, maximum envelope variation, and ripple.	Image representation, IQ samples, RSSI, spectrogram features, power-frequency measurements
Pros	Low implementation cost. Low computational time and complexity	Highly Robust to timing and frequency mismatches. Low computational complexity.	Low implementation cost. Small data sets are sufficient for the algorithm. Low computational time	Minor data preprocessing is required.
Cons	Affected by noise and SNR variation. Require long signal observation time	Accuracy is highly reduced for signals of SNR <2dB.	Require further data preprocessing. Rely on expert knowledge for understanding data structure	High computational complex. Require large amounts of data. Require long signal observation time

C. DMDA IDENTIFICATION SCHEME

Utilizing eigenvalue matrix Λ and DMD modes matrix Φ, DMDA technique calculates a template-features matrix F_x from a set of training samples of a certain technology x. As Fig. 1 illustrates, we projected this matrix on testing samples of different technologies, then we classified the signal by evaluating the resultant DMD mode amplitudes. Utilizing the resultant DMD eigenvalues and modes [32], [37], we arrived at the following:

$$x_i = \Phi \Lambda^i b \tag{12}$$

where, i=1, 2, …, k, and b is a vector containing the coefficients of the initial condition x_1 in the eigenvector basis, such that:

$$b = \Phi^{-1} x_1 \tag{13}$$

From (12), we combine the two terms Φ and Λ^i to define the feature matrix as:

$$F_x = \Phi \Lambda^i \tag{14}$$

Matrix F_x contains unique features of a wireless technology x, which is composed of eigenvalues and eigenmodes. This matrix represents a model describing a specific technology class feature in the DMD domain. DMD modes amplitude can be calculated as:

$$b_t = F_x^{-1} X_t \tag{15}$$

Since b is a vector composed of complex values, we will represent the amplitude by:

$$S_t = b_t \, b_t^* \tag{16}$$

where, t represents a testing sample and b_t^* is the complex conjugate of b_t.

The resulting modes' amplitude determines the detected signal class. Given that they include the same features, subsequent mode amplitude derived from technology x training samples is anticipated to have larger values than other technologies. According to (8), power measurements in X_t affect the values of DMD modes amplitude. Therefore, power measurements of various signals should be at comparable levels. Thus, before using DMDA for classification, signal power must be normalized. Input signals were normalized to a minimum value of zero and a maximum value of one. The pseudo-code of the proposed DMDA technique is given in Algorithm 1.

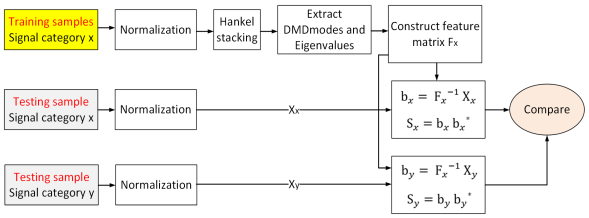

FIGURE 1. DMDA classification scheme outline.

D. DMDF IDENTIFICATION SCHEME

Frequency of the i^{th} DMD mode can be defined as [34], [37]:

$$f_i = |imag(\frac{ln(\lambda_i)}{\Delta t})| \tag{17}$$

f_i represents the absolute oscillation frequency of a DMD mode. The suggested notion recommends comparing the oscillation trend of signals DMD modes, which can be accomplished by rearranging the f_i values for each signal class into descending order and plotting f_ii against an index j, where j=1, 2, 3,…, r. The received signal is then classified using the resulting plots. An overview of the procedure can be found in Fig. 2. To categorize the signals, we used the slope of the ensuing trends. The slope represents the decay of the frequencies of the extracted DMD modes. Algorithm 2 provides a detailed illustration of the suggested technique.

Algorithm 1 Wireless Signal Features Matrix Formation (Matrix F)

Input: signal $y_1, k, m, r, and\ \Delta t$
Output: F

Calculate required number of samples :
$n = m + k - 1$
Extract required signal window:
$Y_1 = y_1(1:n)$
Perform Hankel stacking:
Initialize Y_{11}
for j = 1:m **do**
  $Y_{11} = [Y_{11}\ \ Y_1(:, j : end - m + j)]$
end for
Repeat for all training signals
Combine to form data matrix:
$D = [Y_{11}, Y_{22} \ldots Y_{nn}]^T$
Construct input matrices for DMD:
$X = Y_{11}(:, 1 : end - 1)$
$X' = Y_{11}(:, 2 : end)$
Apply DMD:
$X = U\Sigma V^*$
$U_r = U(:, 1:r)$
$S_r = S(1:r, 1:r)$
$V_r = V(:, 1:r)$
$\tilde{A} = U_r^* X' V_r \Sigma_r^{-1}$
$\tilde{A}W = \Lambda W$
$\Phi = U_r W$
Construct features matrix:
Initialize F
for j = 1:k **do**
  $F = [F; \Phi\Lambda^j]$
end for
*R*epeat for all signals

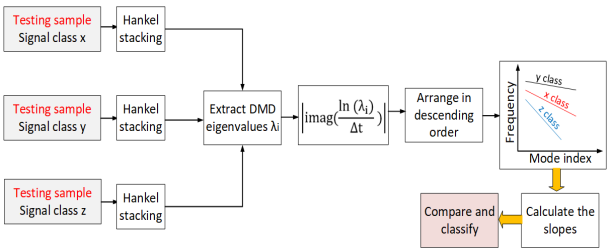

FIGURE 2. DMDF classification scheme outline.

III. DATASETS AND EXPERIMENTAL SETUP

A. ZIGBEE/BLE DATASET

Experimental testing and data collection were conducted at the wireless laboratory at the University of Oklahoma campus in Tulsa. A semi-anechoic chamber was used for testing to eliminate external noise. We set up a heterogeneous wireless network composed of the BLE and ZigBee sub-networks. There were a pair of access point (Tx) and station (Rx) devices in each network. 220 separate—none sharing baseline—raw power timeseries signals of each technology were collected, in addition to 220 coexisting signals in

Algorithm 2 DMDF Scheme

Input: first signal $y_1, k, m, r, and\ \Delta t$
Output: figure

Calculate required number of samples: n=m+k-1
Extract required signal window: $y_1 = y_1(1:n)$
Perform Hankel stacking:
Initialize Y_1
for j = 1:m **do**
  $Y_{11} = [Y_{11}\ \ y_1(:, j : end - m + j)]$
end for
Construct input matrices:
$X = Y_{11}(:, 1 : end - 1)$
$X' = Y_{11}(:, 2 : end)$
Compute SVD of X:
$X = U\Sigma V^*$
$U_r = U(:, 1:r)$
$S_r = S(1:r, 1:r)$
$V_r = V(:, 1:r)$
$\tilde{A} = U_r^* X' V_r \Sigma_r^{-1}$
$\tilde{A}W = \Lambda W$
$\Phi = U_r W$
calculate eigenvalues and oscillation frequencies:
$\lambda_i = diag(\Lambda)$;
$f_i = abs(imag(log(\lambda_i/\Delta t)))$
$f_i = sort(f_i, descend)$; Define index j:
j=[1:1:r];
figure : $Plot(j, f_i)$
*R*epeat for all signals

the 2.4 GHz ISM band. The CC2530 development kit board was used to create ZigBee traffic via channel 14 at a central frequency of 2.42 GHz. We used two laptops equipped with nRF52840-BLE Bluetooth 5.3 chipsets for BLE communication. A National Instruments (NI) vector network analyzer and PXIe-1075 chassis were used to record the transmitted signals' raw power measurements. Power measurements were gathered using a sampling frequency of 500 MHz. Transmitted signals were recorded with an SNR range of 0 to 25dB for various transmitter and receiver locations and heights.

To summarize, 660 timeseries signals containing 10.3 million packets were captured from three scenarios—individual BLE, individual ZigBee, and heterogeneous coexisting BLE and ZigBee—made up the dataset. For each case, we collected 220 signals (i.e., 3.5 million packets). Time domain features of randomly selected signals are shown in Fig. 3.

B. WIFI DATASET

We used a dataset collected by [23] at the wireless laboratory at the Oklahoma University Tulsa campus. For signals with maximum throughputs of 956 Mbps, 340 Mbps, and 250 Mbps, the data set included 450 raw power time series measurements containing 90 million packets for 802.11n, 802.11ac, and 802.11ax, respectively.

TABLE 2. Average values of WIFI signals duty cycles.

DC1	DC2	DC3	DC4	DC5
22%	40%	64%	80%	93%

The collection included individual (or baseline) and coexisted signals in the 5 GHz ISM band with a minimum and constant noise level of less than −73 dBm. There were three different Wi-Fi network setups, each with a pair of access points (Tx) and station (Rx) equipment. To establish an 802.11ax network with 160 MHz of bandwidth on channel 36 (central frequency 5180 MHz), an Asus RT-AX88U device was used. The 802.11n and 802.11ac networks were built using two pairs of MikroTik router boards, and they shared a channel with the 802.11ax network. LabVIEW software was used to extract time domain IQ components from raw power measurements of transmitted signals obtained by NI PXIe-5644R RF vector signal transceiver (VST). The real-time bandwidth IQ sampling rate was set to 10 MS/s. Fig. 4 depicts the time domain properties of randomly selected samples with various duty cycles (DCs) for 20ms time interval. Table 2 shows DC average values.

C. GSM/LTE DATASET

We used a GSM and LTE dataset provided by [38]. The dataset consisted of GSM and LTE signals generated at various SNR levels with a combination of non-line-of-sight (NLOS) and line-of-sight (LOS) conditions. The experiment was performed in the Wireless Research Laboratory in Tubitak, Belgium. Researchers deployed an Agilent vector signal generator (VSG) E4438C as a transmitter. An Agilent PSA series vector signal analyzer (VSA) E4440A was employed as a receiver to capture transmitted signals. The GSM-average received signal strengths ranged from −50 dBm to −45 dBm, while LTE varied between −50 dBm and −40 dBm. Sampling time Δt was set to $0.78\mu s$ and $0.14\mu s$ for GSM and LTE, respectively. Fig. 5 shows various samples of the available time series signals obtained from the dataset.

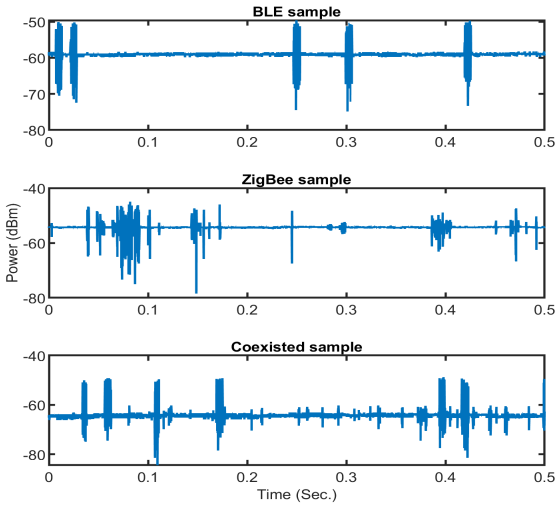

FIGURE 3. Zigbee and BLE Raw power signals.

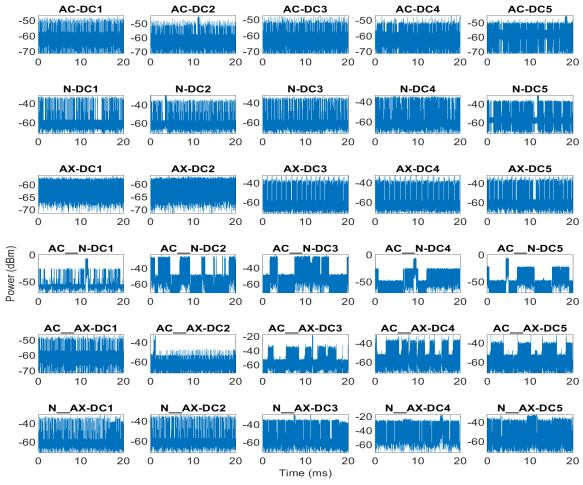

FIGURE 4. Raw power measurements of the collected WIFI signals with various duty cycles.

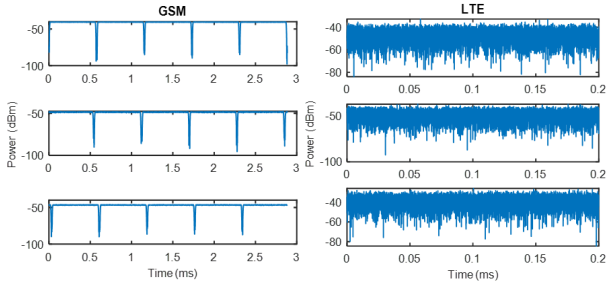

FIGURE 5. Samples of GSM and LTE signals available in the dataset.

IV. SIGNAL FRAME FORMAT AND FEATURES

This section explains the signal model and frame structure of the various wireless technologies included in our analysis. The inherent unique periodicity in each signal, which serves as the algorithm's fundamental property for identification, is highlighted by the frame structure.

A. GSM/LTE

GSM frame structure is a time division multiple access (TDMA). Each frame consists of eight timeslots. Fig. 6 shows timeslot-per-frame for a normal burst [39], which carries encrypted data transmitted between users. We noted the periodicity of the pilot training signals, tail bits (TB), and guard bits (GB). The dedicated 26 bits for the training (i.e., pilot) signal used for channel estimation in each time slot are repeated in the same instance per slot. Since the duration of each timeslot is $577\mu s$, the repetitive frequency of the pilot sequence is 1/577=1733 Hz. Guard and tail (i.e., synchronization) bits have the same value of repetitiveness. Other signaling GSM bursts (i.e., frequency correction, synchronization, and access bursts) have similar repetitive sequences with the same 1733 Hz frequency, although they have a different duration.

Detailed frame structure of LTE FDD downlink can be found in [40] and [41]. Every 10ms LTE frame is divided into 10 subframes, each with 1ms duration. Also, each subframe contains two timeslots (or resource blocks [RBs]) characterized by 0.5ms duration and six or seven OFDM symbols, depending on short- or long-cyclic prefix. The periodicity of various signals demonstrates a constant repetition for the following:

1) Reference/pilot signals (blue): Fixed location along the time axis on the first and fifth OFDM symbol of every RB. These are repeated once per RB (i.e., one time per 0.5ms).
2) PDCCH, PCFICH, PHICH (yellow, red, purple, see below): Exist at the beginning symbol of each subframe and are repeated once per subframe (i.e., one time per 1ms).
3) PSS and SSS (green and orange): Repeated at fixed locations once every 5ms.

where, PDCCH is Physical Downlink Control Channel; PCFICH is Physical Control Format Indicator Channel; PHICH is Physical HARQ Indicator Channel; PSSis Primary Synchronization Signal; and SSS is Secondary Synchronization Signal.

B. WIFI

Highlighting the physical layer (PHY) frame structure of 802.11n, 802.11ac, and 802.11ax Wi-Fi standard signals in the 5 GHz bands, the 802.11 PHY employs bursted packets for transmission. There is a preamble and payload in each packet. Preamble enables synchronization of time and frequency, estimates channel parameters for equalization, and gives receiver header details about the packet, such as configuration, format type, and data rates. Data from the user is transmitted in the payload.

Fig. 7 shows the packet formats for 802.11n, 802.11ac, and 802.11ax Wi-Fi standard signals. The 802.11n high throughput (HT) mixed format begins with legacy preambles: legacy Short Training sequence (L-STF), legacy Long Training sequence (L-LTF), and legacy Signal Description (L-SIG), which can be decoded by legacy 11a/g devices. Legacy preambles are followed by the 11n specific HT preambles, and finally the user data. The 802.11ac frame format has the same beginning legacy preambles, followed by the very high throughput (VHT) preambles, which are unique for 11ac devices.

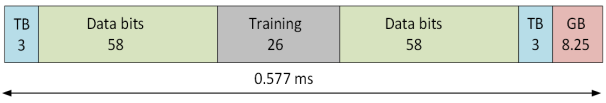

FIGURE 6. GSM timeslot structure for normal burst [23].

Like 11n and 11ac, the 802.11ax packet begins with a traditional preamble followed by a High efficiency (HE) preamble sequence that can only be decoded by 11ax devices. At the end of an 802.11ax frame, a packet extension (PE) with a length of 8 or 16 Bμs can be employed.

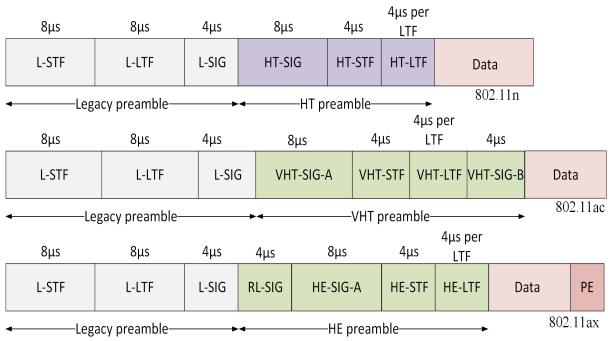

FIGURE 7. 802.11n, 802.11ac, and 802.11ax packet structure.

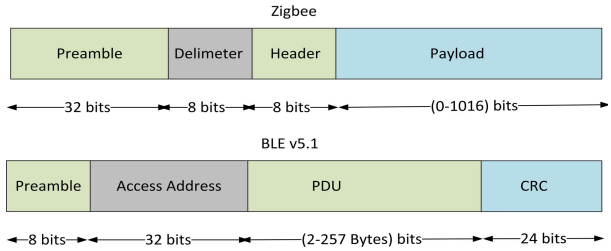

FIGURE 8. Zigbee and BLE packet structure.

C. ZIGBEE/BLE

Data is transmitted via packets by the Zigbee IEEE 802.15.4 PHY. As indicated in Fig. 8, each packet is composed of a preamble (32 bits) for synchronization, the start of packet delimiter (8 bits), physical header (8 bits), and payload segment data unit (0 to 1016 bits) [42]. According to the BLE v5.1 standard created by the Bluetooth SIG, a PHY transmitted packet has four parts: the synchronization preamble (8 bits), access address (32 bits), protocol data unit (PDU)—advertisement or data packet (2-257 octets), and cyclic redundancy check (CRC), which is used to identify packet errors (24 bits) [43].

V. RESULTS AND DISCUSSIONS

A. SELECTION OF DMDA AND DMDF INPUT PARAMETERS

As shown earlier, algorithms 1 and 2 required four input parameters for carrying out the proposed classification algorithm, as follows.

1) Number of snapshots k: Inputting the entire captured raw signal into the algorithm results in unnecessary large computational time. Instead, a minimum number of snapshots (i.e., number of column vectors of data matrices) should be used in data matrix X. Based on the discussion in Section II, for DMD to accurately capture the periodic features embedded in the signals, we must choose an adequate number of snapshots to represent an ample number of packet timeslots. We used the following formula to calculate the required k value:

$$k = \frac{N_{slot}\ T_{slot}}{\Delta t} \tag{18}$$

where, N_{slot} is the number of the standard frame packet duration and T_{slot} is the duration of each packet.

Empirically, we found that N_{slot}=4 was sufficient for DMD to capture repetitive sequence frequencies and assign a signal (See next subsection).

2) Number of stacks m for Hankel matrix formulation: The Hankel matrix number of rows m significantly impacts DMD accuracy. The value of m is dependent on the length of the time series signal n. We found that when m was smaller than n/2 or approximate to n, error increased and accuracy decreased. Therefore, the value of m follows the threshold [34], [37]:

$$n/2 < m < n \tag{19}$$

We chose m to be approximately 60% of the value of n:

$$m = 0.6n \tag{20}$$

3) Truncation value r: The optimal value of r can be found from the inflection point in the decay of the singular values of data matrix X [32], which are the elements of the diagonal matrix Σ of the SVD process. For example, Fig. 9 indicates the decay of the singular values of GSM signal. Singular values were normalized with respect to the first singular value. Based on the inflection point, six modes are ample to represent a GSM signal. This result confirms the significance of DMD, which required only a few numbers of extracted modes (i.e., dominant modes) for identifying a signal.

4) Number of samples n: This parameter represents the length of the timeseries signal, as indicated in (8). The value can be calculated using (4) and (11), given the value of k, as calculated in (18).

B. GSM/LTE IDENTIFICATION

1) APPLYING DMDA TECHNIQUE

This section describes results obtained using DMDA signal identification. DMDA evaluates the resultant DMD mode amplitudes. Fig. 10 shows the resulting modes of two testing samples for a various number of transmitted timeslots (or packets) N_{slot}. The algorithm achieved better distinction as N_{slot} increased. We evaluated six resultant DMD mode amplitudes of GSM and LTE test samples relative to features stored in matrix F, which was constructed using GSM training signals (see Fig. 1). DMD mode amplitudes were evaluated by comparing maximum and average values. As expected, GSM test samples had higher amplitudes than LTE test samples due to common features matching with matrix F. Results confirm the ability of DMDA to identify signals with short time duration (i.e., only 5 packets/timeslots are sufficient). Regarding GSM, N_{slot}=4 was empirically found to sufficiently capture the repetitive sequence frequency, as clearly shown in Fig. 10. Given T_{slot}=577μs and Δt=0.78 μs, k equals approximately 2950. For LTE, N_{slot}=5 was empirically found to capture repetitive sequence frequencies. Given T_{slot}=0.5ms and Δt=0.14 μs, k equals to 17850 approximately.

2) APPLYING DMDF TECHNIQUE

The DMDF identification method classified signals based on evaluating the slope of DMD mode oscillation frequency trend, as explained in Section II. We applied the technique on all the available GSM and LTE samples, and also plotted the oscillation frequency trend for 20 modes (i.e., value of r was set to 40, and then we removed duplicate values, as resultant eigenvalues were complex conjugates). Fig. 11 shows that LTE testing samples had a more pronounced, distinct trend than GSM testing samples (i.e., higher slope). Fig. 11 also shows that only one GSM signal could potentially be misclassified. When observing this signal, it is obvious that the signal contained a high amount of noise when compared with other signals, which affected algorithm accuracy. The absolute value of slope α of the linearly fitted line for modes oscillation frequencies was utilized for identifying each signal class. We developed the identification rule as:

$$\alpha_{LTE} > \alpha_{GSM} \tag{21}$$

where, α_{LTE} and α_{GSM} are the absolute values of slope of the linearly fitted line for modes and their associated oscillation frequencies of LTE and GSM signals, respectively.

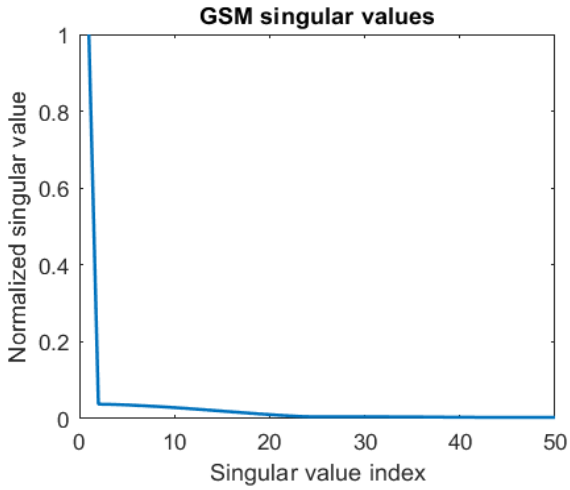

FIGURE 9. Decay of singular values for GSM signal.

3) EVALUATING PERFORMANCE OF DEVELOPED TECHNIQUES

We evaluated DMDF and DMDA technique performance using classification accuracy and processing time required to classify a signal. Concerning DMDA, signals were classified by comparing the maximum value of DMD modes amplitude, as indicated in Fig. 10. GSM signals had higher modes amplitude than LTE signals. Classification accuracy of both GSM and LTE was 90%. The processing time required to identify a signal is approximately 1.5 seconds. The time required to train the DMDA model with four GSM signals was approximately 20 seconds. Employing DMDF scheme, where GSM acquires lower slope than that of LTE, DMDF technique achieved a 90% accurate detection for GSM

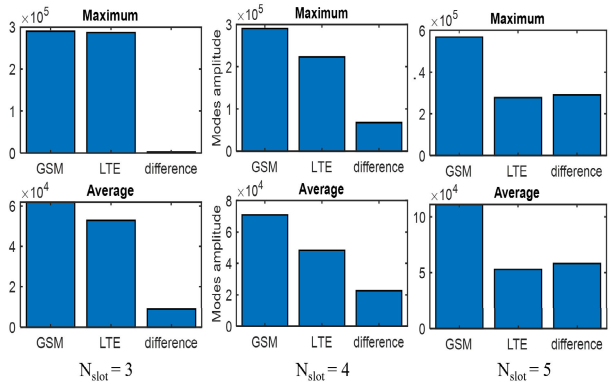

FIGURE 10. Resulted modes amplitudes for testing samples with different values of N_{slot}.

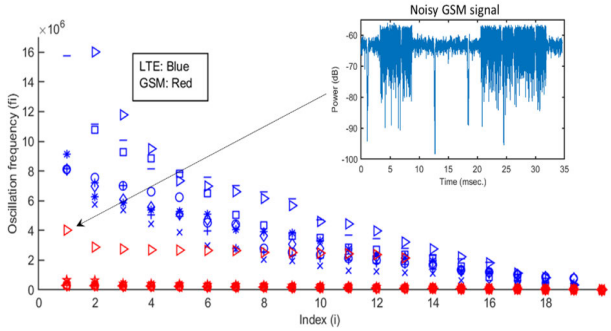

FIGURE 11. Resulted oscillation frequency trend for LTE and GSM signals.

and 100% for LTE. DMDF technique required 3 seconds to identify a signal with no need for training.

Our developed techniques were compared to [7], which utilized second-order cyclostationarity to calculate spectral correlation functions (SCFs). Resulting SCFs were utilized as an input to SVM for classifying various signals, including GSM and LTE. The method achieved 78% accurate detection for GSM and 100% for LTE signals. In addition, we compared the technique's performance with [15] and [16], which distinguished GSM signals from LTE signals by applying CDF analysis using the same dataset used in our analysis. The magnitude of GSM signals follows a Rician distribution, while the magnitude of LTE signals follows a Rayleigh distribution. Using a distribution fitting MATLAB tool and CDF calculation, we classified GSM and LTE based on their CDF. Results achieved 80% accurate detection for GSM and 70 % for LTE. Table 3 provides a comprehensive summary of the overall classification accuracy for the compared techniques. We selected the specific baseline methods for evaluation and comparison due to their relevance in approach and recency to the developed DMDA and DMDF methods. Cyclostationary methods track the periodicity of pilot signals embedded in their transmission. Although this approach is similar to our developed DMDA and DMDF methods, ours requires fewer samples with less complexity to facilitate accurate identification.

TABLE 3. GSM/LTE classification models accuracy.

Technique	DMDA	DMDF	Cyclostationarity	CDF
Accuracy	90%	95%	89%	75%

C. WIFI STANDARD TECHNOLOGY IDENTIFICATION

Classification was performed on both individual (or baseline) and various coexistence scenarios of 802.11n, 802.11ac, and 802.11ax Wi-Fi standard signals in the 5 GHz ISM band. Processed time series raw power signals were collected in a shared heterogeneous deployment [44].

1) INDIVIDUAL SIGNALS IDENTIFICATION

We applied DMDA technique for classifying/differentiating between individual (or baseline) 802.11n, 802.11ac, and 802.11ax Wi-Fi standard signals in the 5 GHz ISM band. Classified signals had the same duty cycle. In the available dataset, each technology contained 25 individual signals divided into five groups. Each group contained five signals having a specific duty cycle (see Table 2). In Fig. 12, we evaluated six resultant DMD mode amplitudes for three random testing samples, regarding features stored in the 802.11ac feature matrix F_{ac}. Mode amplitudes were evaluated by comparing maximum and average values. Fig. 12 indicates that the DMDA technique was able to clearly differentiate between the targeted signals. The 802.11ac signals had the highest amplitudes due to common features matching with the feature matrix F_{ac}. The 802.11n signals had lower amplitude than 802.11ac, while the 802.11ax signals had the lowest amplitude. We empirically developed the identification rule expressed as:

$$S_{ac} > S_n > S_{ax} \tag{22}$$

where, S_{ac}, S_n, and S_{ax} are the maximum mode amplitude for Wi-Fi-802.11ac, 802.11n, and 802.11ax signals, respectively.

Applying DMDF on the same dataset for each signal, we plotted the oscillation frequencies for 16 modes. Fig. 13 shows the resulted modes oscillation frequencies of a randomly chosen signal for each duty cycle. More specifically, the absolute value of slope α of the linearly fitted line for modes oscillation frequencies (or dashed line) was utilized for identifying each signal category. As Fig. 13 indicates, the identification rule for all duty cycles can be defined as:

$$\alpha_{ac} > \alpha_n > \alpha_{ax} \tag{23}$$

where, α_{ac}, α_n, and α_{ax} are the absolute value of slope from the linearly fitted line for modes oscillation frequencies of Wi-Fi-802.11ac, 802.11n, and 802.11ax signals, respectively. This result indicated that the DMDF technique can extract unique features and accurately classify targeted signals.

2) COEXISTING SIGNALS IDENTIFICATION

We created five coexistence scenarios, each coexisting two Wi-Fi signals having the same duty cycle. Each scenario was repeated according to the duty cycles provided in Table 2.

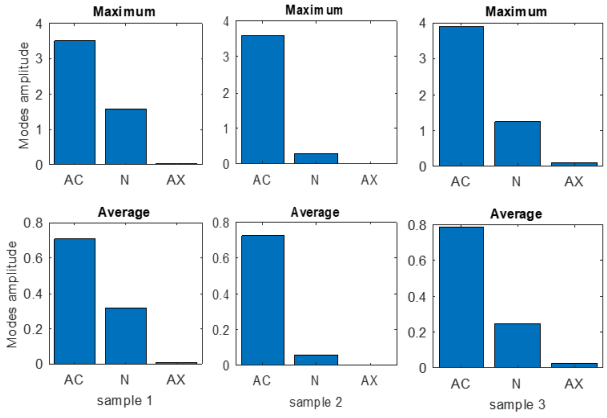

FIGURE 12. Individual Wi-Fi signals identification employing DMDA.

We applied a DMDF technique to differentiate between coexisting signals and individual signals of the same Wi-Fi technology. Figs. 14, 15, and 16 compared the resulted modes oscillation frequencies of a randomly chosen signal from each coexistence scenario with individual signals having the same duty cycle. The slope of the linearly fitted line for modes oscillation frequencies (see dashed line) demonstrates that the coexisted signal has the lowest slope of all cases. On the other hand, DMDA was able to classify ac, n, and coexisted ac-n signals. However, DMDA was not able to differentiate between ax and coexisted signals containing ax (e.g., coexisted ax-ac and ax-n signals) as they had similar amplitude values without enough separating margin for accurate classification.

3) PERFORMANCE EVALUATION

DMDA classified the signals by thresholding the maximum value of DMD modes amplitude. DMDF classified the signals by thresholding the values of slopes. Selected thresholding values are indicated in Table 4.

Regarding individual signals classification, DMDA technique correctly classified ac signals with 84% accuracy, n signals with 88% accuracy, and ax signals with 92% accuracy. DMDF achieved better accuracy, as it correctly classified signals with overall accuracy of 98.6 %. DMDF classification accuracy of n, ac, and ax signals was 96%, 100%, and 100%, respectively. On the other hand, while classifying individual and coexisted signals of the same technology (as Figs. 16, 17, and 18 indicated), DMDF technique achieved 93.3% accuracy for classifying n, ac, and coexisted n-ac signals; 93.3% for classifying n, ax, and coexisted n-ax signals, and 97.3% for classifying ax, ac, and coexisted ax-ac signals. DMDA was able to classify n, ac, and coexisted n-ac signals with accuracy of 82%.

CNN, ResNet, and WaveNet are indicative of recently studied and published deep learning architectures used for wireless signal identification. This type of approach is somewhat relevant to our developed algorithms since data training and model development are part of our approach. Hence, we selected the aforementioned models to compare and

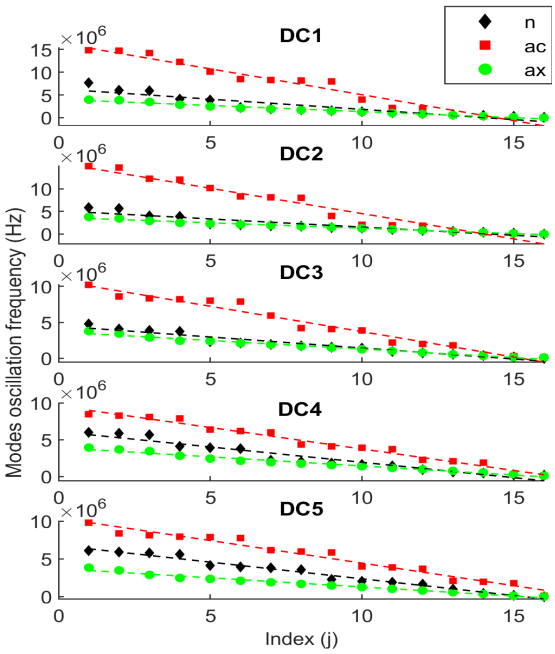

FIGURE 13. Individual Wi-Fi signals identification employing DMDF.

TABLE 4. Threshold values used for signals classification.

DMDA threshold	DMDF threshold	Class
S < 0.1	220,000 <α< 280,000	ax
0.1 < S < 1.5	280,000 <α< 550,000	n
S > 1.5	α > 550,000	ac
-	α < 220,000	Coexisted signals

evaluate our developed DMDA with DMDF techniques. Comparing obtained results with the WaveNet deep learning model performed in [23], researchers achieved lower classification accuracies of 96%, 98%, and 98% for n, ac, and ax individual signals. For coexisted signals, their technique achieved 90% accuracy for classifying coexisted ax-n and 91% for coexisted ax-ac signals. The proposed DMDF technique not only achieved higher accuracy but also, the computational time was extensively reduced by approximately 85%.

In addition, a developed CNN architecture and ResNet9 CNN model [45] were trained to classify the collected signals. We utilized gramian angular summation field (GASF) transformation [46] to extract features. GASF was utilized to encode the collected, one-dimensional (1D) raw power timeseries signals into two-dimensional (2D) texture images for inputting into CNN classifier models. Generated images were 300 × 300 pixels. Because signal power measurements are distinct and to alleviate the effect of diverse SNR values between technologies, a preprocessing normalization step was performed on signals before applying the transformation. Training was conducted on 50% of the dataset (see section III) for both individual and coexisting scenarios. with batch size of eight images using a cross-entropy loss function along with an Adagrad optimizer [47]. Learning rate was set to 0.001. Models were implemented, trained, and

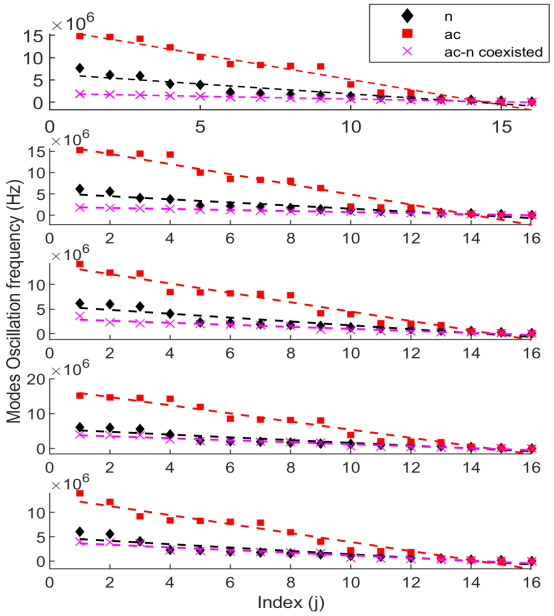

FIGURE 14. Identifying coexisted ac-n Wi-Fi signals employing DMDF.

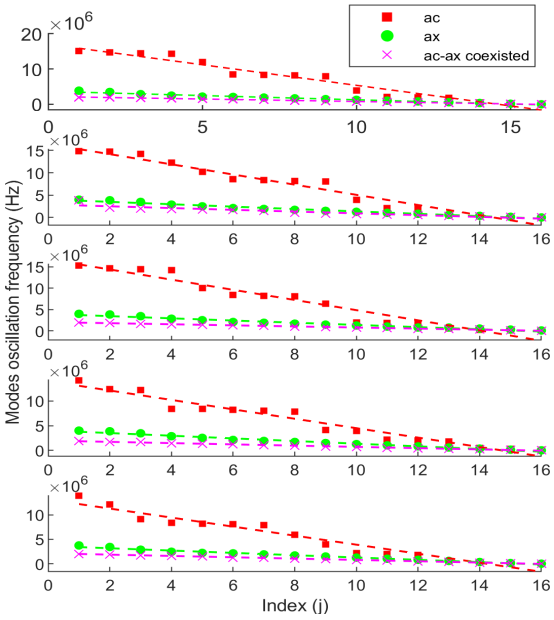

FIGURE 15. Identifying coexisted ac-ax Wi-Fi signals employing DMDF.

tested in the open-source Pytorch software library. The developed CNN was structured with six transformation layers, and the network was convolutional with batch normalization and ReLU activation layers, a pooling layer, and dense fully connected (FC) layers. The final FC layer was the output layer, which computes scores for each of the three class labels. The label with the highest score was the one predicted by the model. Fig. 17 depicts the complete network structure and Kernel filter sizes K.

Table 5 evaluated and compared model performance in terms of overall classification accuracy, processing time required to identify a signal, and model training time.

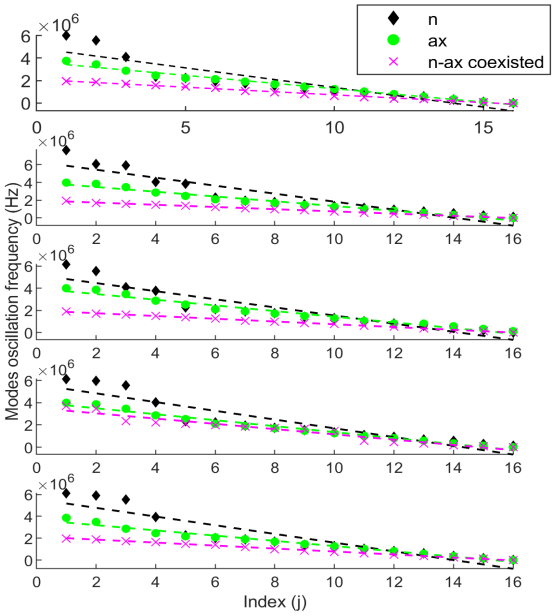

FIGURE 16. Identifying coexisted n-ax Wi-Fi signals employing DMDF.

For CNN models, the best accuracy was attained for 50 epochs. It should be noted that CNN models are expected to have higher accuracy for larger training samples when compared with the sample trained and reported herein. However, this will be at the expense of additional time required to train the models.

D. ZIGBEE-BLE IDENTIFICATION

We proposed DMDA and DMDF techniques to classify individual (i.e., none sharing baseline) and coexistence scenarios for experimentally collected BLE and Zigbee signals in a shared heterogeneous deployment in the 2.4 GHz ISM band [48].

1) APPLYING DMDA AND DMDF SCHEME

In Fig. 18, we evaluated six resultant DMD mode amplitudes for three random testing samples with regard to features stored in the Zigbee feature matrix F_z. Mode amplitudes were evaluated by comparing maximum and average values. Fig. 18 indicates that DMDA technique was able to clearly differentiate between the targeted signals. As expected, ZigBee test samples had the highest amplitudes due to common features with F_z. BLE test signals had lower amplitude than ZigBee; the coexisted signal had the lowest amplitude. We empirically developed the identification rule expressed as:

$$S_{zig.} > S_{BLE} > S_{co} \tag{24}$$

where, $S_{zig.}$, S_{BLE}, and S_{co} are the maximum mode amplitude for ZigBee, BLE, and coexisted ZigBee/BLE signals, respectively.

In Fig. 19 we plotted the oscillation frequency trend for 10 unique modes based on two randomly chosen dataset samples. Each technology had a pronounced, distinct trend

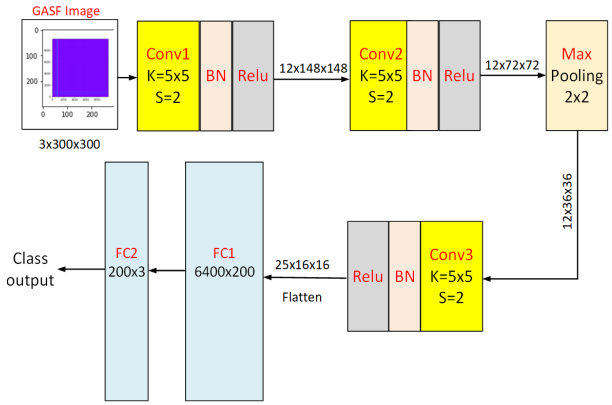

FIGURE 17. CNN network developed for classifying ISM band wireless signals.

TABLE 5. Performance evaluation for various implemented models.

Model	Overall Accuracy (individual)	Overall Accuracy (coexisted)	Processing time	Training time
DMDA	88%	82%	0.5 sec.	1 min.
DMDF	98.6%	94.6%	3 sec.	no training required
WaveNet	97.3%	91%	0.4 sec.	14 hrs
CNN	71%	70%	2 sec.	6 min.
ResNet9	80%	78%	2.5 sec.	20 min.

(i.e., slope). We empirically developed the identification rule expressed as:

$$\alpha_{zig.} > \alpha_{BLE} > \alpha_{co} \tag{25}$$

where, $\alpha_{zig.}$, α_{BLE}, and α_{co} are the absolute value of slope from the linearly fitted line for modes oscillation frequencies ZigBee, BLE, and coexisted ZigBee/BLE signals, respectively.

2) PERFORMANCE EVALUATION

Concerning DMDA, signals were classified by thresholding the maximum value of DMD modes amplitude, as indicated in Table 6. The technique correctly classified signals with overall accuracy of 86.3%. Classification accuracy of ZigBee, BLE, and coexisted signals was 86%, 81%, and 91%, respectively.

Applying DMDF, signals were classified by thresholding values of the slopes, as indicated in Table 6. DMDF acheived an overall classification accuracy of 87.6%. Classification accuracy of ZigBee, BLE, and coexisted signals was 91%, 85.5%, and 86.4%, respectively.

We evaluated the performance of DMDA and DMDF techniques using overall classification accuracy, processing time required to identify a signal, and model training time. Both techniques were compared with the developed CNN model and ResNet-9 model for validation (see subsection C). CNN-based models training was conducted on 50% of the dataset with a batch size of eight images using a cross-entropy loss function along with an Adagrad optimizer. The learning rate was set to 0.001. The accuracy of all models was calculated using the same set of testing samples. Table 7 provided a comparison of the performance of the implemented models.

Results showed that the developed DMD-based techniques achieved high performance for classifying various individual and coexisted wireless signals. In most cases analyzed for this paper, DMD-based techniques had the advantage of high accuracy and short training/processing time required to identify a signal when compared to other techniques. The DMDF scheme outperformed all compared techniques and did not require training. DMDF also achieved the highest accuracy and shortest processing time for identifying a signal.

E. COMPUTATIONAL COMPLEXITY

Four algorithms (CNN, ResNet, WaveNet, and cyclostationary) were implemented to confirm the computational advantage of our developed techniques over others. DMDA/DMDF computational complexity was attributed to the SVD calculation [32]. Notably, our algorithm was successfully implemented using a truncated SVD solution. Doing so limited its complexity to $O(rn^2)$. Truncation value r was less than 10, and n was limited to less than five wireless packet samples. However, the implemented 3-layer CNN model complexity was $O(knd^2)$ per convolutional layer, where d is the layer dimension [49]. Furthermore, the implemented 9-layer ResNet complexity was $O(knd^2)$ per layer. Additionally, the implemented WaveNet had a very high exponential complexity $O(2^L)$, where L is the number of layers of the

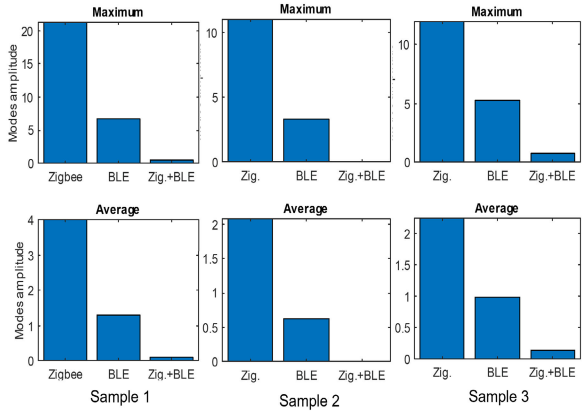

FIGURE 18. ZigBee-BLE identification employing DMDA scheme.

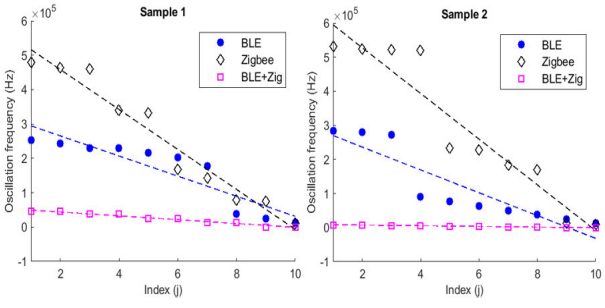

FIGURE 19. ZigBee-BLE identification employing DMDF scheme.

network (i.e., large number) [50]. Finally, cyclostationary complexity was O(2n[4 + 2log2h + 4n + 2h + hlog2(4n/h)]), where h is the FFT number of points [1]. In comparison, our approach required fewer signal samples and achieved higher accuracy with less computational time, as shown in Tables 5 and 7.

TABLE 6. Threshold values used for ZigBbee/BLE classification.

DMDA threshold	DMDF threshold	Class
10 < S < 30	33,000 <α< 70,000	ZigBee
2 < S < 8	11,000 <α< 31,000	BLE
0.01 < S < 1	900 <α< 9,000	coexisted
-	α < 220,000	Coexisted signals

TABLE 7. Performance evaluation for various implemented models.

Model	Overall Accuracy	Processing time	Training time
DMDA	86.3%	0.5 sec.	1 min.
DMDF	87.6%	3 sec.	no training required
CNN	72%	2.1 sec	12 min.
ResNet9	80%	2.5 sec.	40 min.

VI. CONCLUSION

Wireless identification technologies and effective coexistence management are desperately needed, as the number of wireless technologies operating in both licensed and unlicensed bands continues to increase. The research highlighted in this paper reports the development of two novel techniques for wireless technology identification, namely DMDA and DMDF, which are the first to employ a DMD algorithm for identifying signals. Our identification algorithms are based on capturing periodic features embedded in targeted signals by utilizing a DMD mathematical platform. The DMDA technique is based on evaluating a template-features matrix obtained for a specific signal class, and then classifying signals under evaluation according to the values of the resulting projected DMD mode amplitude. The DMDF technique classifies signals based on evaluating the slope of the DMD modes oscillation frequency trend. The proposed techniques were implemented on experimental datasets captured under various channel conditions. When compared with various similar techniques implemented in the literature, results showed that DMD-based algorithms had lower complexity and achieved higher performance. The algorithms can differentiate and classify wireless signals with high accuracy by employing short observation intervals (e.g., four-time slots or packets), which enable them to be implemented in real-time for identifying various operating wireless technologies coexisting in heterogeneous networks. DMDF scheme outperformed all compared techniques, as it is a direct identification scheme (i.e., no training required). This technique achieved the highest accuracy—greater than 90% for most cases—and the shortest time required to identify a signal—less than one second. The proposed DMD-based identification algorithms showed promising performance in accurately identifying three wireless technologies simultaneously operating in the same environment. In future work, the authors would like to evaluate the scalability of the algorithms to track more networks with more diverse coexistence scenarios.

REFERENCES

[1] K. Tekbiyik, O. Akbunar, A. R. Ekti, A. Gorcin, and G. K. Kurt, "Multi–dimensional wireless signal identification based on support vector machines," *IEEE Access*, vol. 7, pp. 138890–138903, 2019.

[2] X. Li, F. Dong, S. Zhang, and W. Guo, "A survey on deep learning techniques in wireless signal recognition," *Wireless Commun. Mobile Comput.*, vol. 2019, pp. 1–12, Feb. 2019.

[3] N. Kato, B. Mao, F. Tang, Y. Kawamoto, and J. Liu, "Ten challenges in advancing machine learning technologies toward 6G," *IEEE Wireless Commun.*, vol. 27, no. 3, pp. 96–103, Jun. 2020.

[4] G. Naik, J. Liu, and J.-M. Park, "Coexistence of wireless technologies in the 5 GHz bands: A survey of existing solutions and a roadmap for future research," *IEEE Commun. Surveys Tuts.*, vol. 20, no. 3, pp. 1777–1798, 3rd Quart., 2018.

[5] N. Bitar, S. Muhammad, and H. H. Refai, "Wireless technology identification using deep convolutional neural networks," in *Proc. IEEE 28th Annu. Int. Symp. Pers., Indoor, Mobile Radio Commun. (PIMRC)*, Oct. 2017, pp. 1–6.

[6] S. Sun, L. Gong, B. Rong, and K. Lu, "An intelligent SDN framework for 5G heterogeneous networks," *IEEE Commun. Mag.*, vol. 53, no. 11, pp. 142–147, Nov. 2015.

[7] K. Tekbiyik, O. Akbunar, A. R. Ekti, G. K. Kurt, and A. Gorcin, "On the investigation of wireless signal identification using spectral correlation function and SVMs," in *Proc. IEEE Wireless Commun. Netw. Conf. (WCNC)*, Marrakesh, Morocco, Apr. 2019, pp. 1–5.

[8] C. Skiribou and F. Elbahhar, "V2X wireless technology identification using time–frequency analysis and random forest classifier," *Sensors*, vol. 21, no. 13, p. 4286, Jun. 2021.

[9] B. Liu and K. C. Ho, "Identification of CDMA signal and GSM signal using the wavelet transform," in *Proc. 42nd Midwest Symp. Circuits Syst.*, Las Cruces, NM, USA, Aug. 1999, pp. 678–681.

[10] K. C. Ho, H. Liu, and L. Hong, "On improving the accuracy of a wavelet based identifier to classify CDMA signal and GSM signal," in *Proc. IEEE Int. Symp. Circuits Syst. VLSI*, Orlando, FL, USA, May 1999, pp. 564–567.

[11] M. Oner and F. Jondral, "Cyclostationarity based air interface recognition for software radio systems," in *Proc. IEEE Radio Wireless Conf.*, Atlanta, GA, USA, Sep. 2004, pp. 263–266.

[12] E. Karami, O. A. Dobre, and N. Adnani, "Identification of GSM and LTE signals using their second-order cyclostationarity," in *Proc. IEEE Int. Instrum. Meas. Technol. Conf. (I2MTC)*, Pisa, Italy, May 2015, pp. 1108–1112.

[13] M. Kulin, T. Kazaz, I. Moerman, and E. De Poorter, "End-to-end learning from spectrum data: A deep learning approach for wireless signal identification in spectrum monitoring applications," *IEEE Access*, vol. 6, pp. 18484–18501, 2018.

[14] G. C. Zanuz, J. M. Winter, I. Müller, J. L. T. Garzon, J. C. Netto, and C. E. Pereira, "Identification of IEEE 802.11 g and IEEE 802.15.4 signals using energy and cyclostationarity detection approach," in *Proc. 1st Int. Symp. Instrum. Syst., Circuits Transducers (INSCIT)*, Belo Horizonte, Brazil, Aug. 2016, pp. 55–60.

[15] Y. A. Eldemerdash, O. A. Dobre, O. Ureten, and T. Yensen, "Fast and robust identification of GSM and LTE signals," in *Proc. IEEE Int. Instrum. Meas. Technol. Conf. (I2MTC)*, Turin, Italy, May 2017, pp. 1–6.

[16] Y. A. Eldemerdash, O. A. Dobre, O. Üreten, and T. Yensen, "Identification of cellular networks for intelligent radio measurements," *IEEE Trans. Instrum. Meas.*, vol. 66, no. 8, pp. 2204–2211, Aug. 2017.

[17] H. Xia, K. Alshathri, V. B. Lawrence, Y.-D. Yao, A. Montalvo, M. Rauchwerk, and R. Cupo, "Cellular signal identification using convolutional neural networks: AWGN and Rayleigh fading channels," in *Proc. IEEE Int. Symp. Dyn. Spectr. Access Netw. (DySPAN)*, Nov. 2019, pp. 1–5.

[18] K. Alshathri, H. Xia, V. Lawrence, and Y.-D. Yao, "Cellular system identification using deep learning: GSM, UMTS and LTE," in *Proc. 28th Wireless Opt. Commun. Conf. (WOCC)*, Beijing, China, May 2019, pp. 1–4.

[19] H. Gu, Y. Wang, S. Hong, Y. Xu, and G. Gui, "Deep learning based intelligent recognition method in heterogeneous communication networks," in *Proc. IEEE/CIC Int. Conf. Commun. China (ICCC)*, Chongqing, China, Aug. 2020, pp. 478–482.
[20] M. Schmidt, D. Block, and U. Meier, "Wireless interference identification with convolutional neural networks," in *Proc. IEEE 15th Int. Conf. Ind. Informat. (INDIN)*, Emden, Germany, Jul. 2017, pp. 478–482.
[21] J. Fontaine, E. Fonseca, A. Shahid, M. Kist, L. A. DaSilva, I. Moerman, and E. De Poorter, "Towards low-complexity wireless technology classification across multiple environments," *Ad Hoc Netw.*, vol. 91, Aug. 2019, Art. no. 101881.
[22] E. Almazrouei, G. Gianini, N. Almoosa, and E. Damiani, "Robust computationally-efficient wireless emitter classification using autoencoders and convolutional neural networks," *Sensors*, vol. 21, no. 7, p. 2414, Apr. 2021.
[23] R. J. Estes, D. Willis, and H. H. Refai, "Classifying Wi-Fi from raw power measurements using a neural network adapted from WaveNet," in *Proc. IEEE Int. Conf. Commun.*, Montreal, QC, Canada, Jun. 2021, pp. 1–6.
[24] J. Gong, X. Qin, and X. Xu, "Multi-task based deep learning approach for open-set wireless signal identification in ISM band," *IEEE Trans. Cognit. Commun. Netw.*, vol. 8, no. 1, pp. 121–135, Mar. 2022.
[25] M. He, S. Peng, H. Wang, and Y.-D. Yao, "Identification of ISM band signals using deep learning," in *Proc. 29th Wireless Opt. Commun. Conf. (WOCC)*, May 2020, pp. 1–4.
[26] H. S. Ghanem, R. M. Al-Makhlasawy, W. El-Shafai, M. Elsabrouty, H. F. A. Hamed, G. M. Salama, and F. E. A. El-Samie, "Wireless modulation classification based on radon transform and convolutional neural networks," *J. Ambient Intell. Humanized Comput.*, vol. 2022, pp. 1–10, May 2022.
[27] C. T. Fredieu, A. Martone, and R. M. Buehrer, "Open-set classification of common waveforms using a deep feed-forward network and binary isolation forest models," in *Proc. IEEE Wireless Commun. Netw. Conf. (WCNC)*, Austin, TX, USA, Apr. 2022, pp. 2465–2469.
[28] K. S. Durbha and S. Amuru, "AutoML models for wireless signals classification and their effectiveness against adversarial attacks," in *Proc. 14th Int. Conf. Commun. Syst. Netw. (COMSNETS)*, Bangalore, India, Jan. 2022, pp. 265–269.
[29] L.-X. Wang and Y.-J. Ren, "Recognition of digital modulation signals based on high order cumulants and support vector machines," in *Proc. ISECS Int. Colloq. Comput., Commun., Control, Manage.*, Sanya, China, Aug. 2009, pp. 271–274.
[30] X. Wang, Z. Gao, Y. Fang, S. Yuan, H. Zhao, W. Gong, M. Qiu, and Q. Liu, "A signal modulation type recognition method based on kernel PCA and Random Forest in cognitive network," in *Proc. Int. Conf. Intell. Comput.*, 2014, pp. 522–528.
[31] S. Grimaldi, A. Mahmood, and M. Gidlund, "Real-time interference identification via supervised learning: Embedding coexistence awareness in IoT devices," *IEEE Access*, vol. 7, pp. 835–850, 2019.
[32] J. N. Kutz, S. L. Brunton, B. W. Brunton, and J. L. Proctor, *Dynamic Mode Decomposition: Data-Driven Modeling of Complex Systems*. Philadelphia, PA, USA: SIAM, 2016. Accessed: Jan. 28, 2022, doi: 10.1137/1.9781611974508.
[33] Z. Wu, D. Laurence, S. Utyuzhnikov, and I. Afgan, "Proper orthogonal decomposition and dynamic mode decomposition of jet in channel crossflow," *Nucl. Eng. Des.*, vol. 344, pp. 54–68, Apr. 2019.
[34] P. J. Schmid, "Dynamic mode decomposition of numerical and experimental data," *J. Fluid Mech.*, vol. 656, pp. 5–28, Jan. 2010.
[35] A. A. Kaptanoglu, K. D. Morgan, C. J. Hansen, and S. L. Brunton, "Characterizing magnetized plasmas with dynamic mode decomposition," *Phys. Plasmas*, vol. 27, no. 3, Mar. 2020, Art. no. 032108.
[36] K. Fujii and Y. Kawahara, "Dynamic mode decomposition in vector-valued reproducing kernel Hilbert spaces for extracting dynamical structure among observables," *Neural Netw.*, vol. 117, pp. 94–103, Sep. 2019.
[37] S. Zhou, G. Lin, Q. Qian, and C. Xu, "Binary classification of floor vibrations for human activity detection based on dynamic mode decomposition," *Neurocomputing*, vol. 432, pp. 227–239, Apr. 2021.
[38] O. Akbunar, A. R. Ekti, G. K. Kurt, and A. Görc. *Standard-Based Wireless Signals*. Accessed: Feb. 2022. [Online]. Available: https://data.mendeley.com/datasets
[39] *GSM Technical Specification*. Accessed: Jan. 2022. [Online]. Available: https://www.etsi.org/committee/3gpp
[40] *LTE Frame Structure Made Simple*. Accessed on: Jan. 2022. [Online]. Available: https://ourtechplanet.com/lte-frame-structure-made-simple/
[41] S.-W. Kim and K.-Y. Kim, "Physical layer verification for 3GPP LTE (FDD)," in *Proc. 11th Int. Conf. Adv. Commun. Technol.*, 2009, pp. 1095–1100.
[42] L. Chaari and L. Kamoun, "Performance analysis of IEEE 802.15.4/ZigBee standard under real time constraints," *Int. J. Comput. Netw. Commun.*, vol. 3, no. 5, pp. 235–251, Sep. 2011.
[43] *Bluetooth Low Energy—It Starts With Advertising*. Accessed: Apr. 2021. [Online]. Available: https://www.bluetooth.com/blog/
[44] A. Elsebaay and H. H. Refai, "Wi-Fi standard technology identification employing dynamic mode decomposition modeling," in *Proc. IEEE Global Commun. Conf.*, Rio de Janeiro, Brazil, Dec. 2022, pp. 4788–4793.
[45] *Using ResNet for Image Classification*. Accessed: Mar. 2021. [Online]. Available: https://blog.jovian.ai/using-resnet-for-image-classification-4b3c42f2a27e
[46] C.-L. Yang, C.-Y. Yang, Z.-X. Chen, and N.-W. Lo, "Multivariate time series data transformation for convolutional neural network," in *Proc. IEEE/SICE Int. Symp. Syst. Integr. (SII)*, Paris, France, Jan. 2019, pp. 188–192.
[47] J. Duchi, E. Hazan, and Y. Singer, "Adaptive subgradient methods for online learning and stochastic optimization," *J. Mach. Learn. Res.*, vol. 12, no. 7, pp. 1–39, 2011.
[48] A. Elsebaay and H. H. Refai, "Identifying coexisting Bluetooth and ZigBee technologies employing dynamic mode decomposition," in *Proc. IEEE Globecom Workshops*, Rio de Janeiro, Brazil, Dec. 2022, pp. 432–437.
[49] A. Vaswani, N. Shazeer, N. Parmar, J. Uszkoreit, L. Jones, A. N. Gomez, and I. Polosukhin, "Attention is all you need," in *Proc. Adv. Neural Inf. Process. Syst.*, vol. 30, 2017, pp. 1–16.
[50] S. Hussain, M. Javaheripi, P. Neekhara, R. Kastner, and F. Koushanfar, "FastWave: Accelerating autoregressive convolutional neural networks on FPGA," in *Proc. IEEE/ACM Int. Conf. Comput.-Aided Design (ICCAD)*, Nov. 2019, pp. 1–8.

AHMED ELSEBAAY received the B.Sc. degree in electrical power and machine engineering and the M.Sc. degree in electrical engineering from Helwan University, Cairo, Egypt, in May 2012 and May 2018, respectively. He is currently pursuing the Ph.D. degree in electrical and computer engineering with The University of Oklahoma, Tulsa, OK, USA. From 2013 to 2019, he worked as a Research Assistant with the Faculty of Engineering, Helwan University. From 2019 to 2020, he also worked as a Researcher with the Public University of Navarra, Pamplona, Spain. Since 2020, he has been with The University of Oklahoma, where he is also working on multiple research projects focusing on wireless coexistence, signal processing, mathematical modeling, machine learning, and deep learning. His research interests include the Internet of Things and data collection by deploying wireless sensor networks.

HAZEM H. REFAI (Member, IEEE) is currently the Williams Chair of Telecommunication and Networking with the School of Electrical and Computer Engineering (ECE) Telecommunication Program, The University of Oklahoma-Tulsa (OU-Tulsa), Tulsa, OK, USA, where he is also the Founder and the Director of the Wireless Electromagnetic Compliance and Design (WECAD) Center. WECAD's mission is to conduct basic and applied research examining wireless coexistence. He has published more than 190 refereed papers for national and international conferences and journal articles. His research interests include the development of optical wireless communication, physical and medium access control layers to enhance wireless coexistence, and cognitive radios and networks. He is the past IEEE ComSoc Tulsa Chapter President and served as the Organization's North American Distinguished Lecturer Tour Coordinator.